Journal of Materiomics 8 (2022) 221–228

Contents lists available at ScienceDirect

Journal of Materiomics

journal homepage: www.journals.elsevier.com/journal-of-materiomics/

Facile synthesis of iron–nickel–cobalt ternary oxide (FNCO) mesoporous nanowires as electrode material for supercapacitor application

Muhammad Usman [a, b], Muhammad Tayyab Ahsan [b], Sofia Javed [a], Zeeshan Ali [a], Yiqiang Zhan [c], Irfan Ahmed [c], Sajid Butt [d], Mohammad Islam [e], Asif Mahmood [f, **], M. Aftab Akram [a, *]

[a] School of Chemical and Materials Engineering, National University of Sciences and Technology (NUST), Sector H-12, Islamabad, 44000, Pakistan
[b] Department of Materials Science and Engineering, College of Engineering, Peking University, 100871, Beijing, China
[c] State Key Laboratory of ASIC and System, Center of Micro-Nano System, SIST, Fudan University, Shanghai, 200433, China
[d] Department of Materials Science and Engineering, Institute of Space Technology, Islamabad, 44000, Pakistan
[e] New Mexcico Institute of Mining & Technology, Socorro, NM 87801, USA
[f] School of Chemical and Biomolecular Engineering, The University of Sydney, 2006, Sydney, Australia

ARTICLE INFO

Article history:
Received 17 January 2021
Received in revised form
3 March 2021
Accepted 16 March 2021
Available online 21 March 2021

Keywords:
Electrochemistry
Hydrothermal synthesis
Nanowires
Supercapacitor
Transition metal oxides

ABSTRACT

Transition Metal Oxides have drawn significant attention due to their reversible chemical redox reaction and long-life stability. Inexorable agglomeration and shrinkage/expansion of transition metal oxides in the nanosize regime have a noticeable effect on their electrochemical properties. Here in this work, mesoporous nanowires (NWs) with a typical composition of iron-nickel-cobalt ternary oxide (FNCO) are synthesized using a simple, facile and cost-effective hydrothermal process followed by furnace annealing. These NWs are then extensively investigated as an electrode material for supercapacitor application. To compare the electrochemical properties, nanowires of nickel-cobalt oxide (NCO), iron-cobalt oxide (FCO) and cobalt oxide (CO) were also produced by following the same protocol. The FNCO NWs are found to overcome the shortcomings in the electrochemical energy storage devices by exhibiting higher values of specific capacitance (2197 Fg^{-1}) and energy density (109 $Whkg^{-1}$) at 1 Ag^{-1} current rate. Moreover, the FNCO NWs also showed a cyclic charge/discharge stability of 96% even up to 20,000 cycles. Furthermore, a FNCO//graphene asymmetric device, fabricated with FNCO NWs and graphene as positive and negative electrodes, respectively, which exhibit high energy density (47 $Whkg^{-1}$), power density (375 Wkg^{-1}) and excellent capacitance retention (86%) after 15,000 cycles.

1. Introduction

The rapidly growing energy crisis in the world has prompted scientists and industrialists to make intensive efforts for the development of new materials and technologies to fulfill high energy and power demands. The difference between energy demand and supply can only be reduced through the use of renewable energy resources such as hydroelectric, biomass, photocatalysis, wind, waves, geothermal and photovoltaics, most of which produce electric power intermittently [1–9]. Hence, the coupling of these resources with highly efficient energy storage devices is vital. In this regard, supercapacitors with high power density, fast charge-discharge rate and long life cycle stability have become the most promising type of energy storage devices [10–15]. Since, the performance of these devices primarily relies on the electrode materials [16], different strategies have been explored to achieve the best performance of energy storage media. The two main contenders for energy storage applications are batteries and supercapacitors. Although the batteries store more energy using faradaic redox reaction [17], the supercapacitors works on the principle of charge accumulation in the electrochemical double layer and yield high power density [18]. Nowadays, with the evolution of the

* Corresponding author.
** Corresponding author.
E-mail addresses: asif.mahmood@sydney.edu.au (A. Mahmood), aftabakram@scme.nust.edu.pk (M.A. Akram).
Peer review under responsibility of The Chinese Ceramic Society.

https://doi.org/10.1016/j.jmat.2021.03.012

asymmetric/hybrid supercapacitor devices, the differences between batteries and supercapacitors have been blurred, as these type of devices use both types of the phenomenon during their operation [19–24]. However, the performance of these devices is still far from commercial applications. The performance of supercapacitor devices is largely determined by electrode chemistries. Hence, various electrode chemistries including carbonaceous and metallic (*e.g.* MnO_2, Co_3O_4, $ZnCo_2O_4$, $CuCo_2O_4$ *etc.*) have been investigated for their charge storage capabilities [16,25–32]. The high resistivity of transition metal oxides (TMOs) is big hurdle for their applications in supercapacitors. The electrical properties of TMOs can be improved by introducing defects or impurities via selected gaseous environment or through doping. Among all the transition metals, cobalt (Co) based oxides has found widespread use as electrode material in supercapacitors and batteries owing to its high theoretical specific capacitance, energy density and long runtime [33]. More recently, cobalt oxide (Co_3O_4) with different nanoscale morphologies and/or as hybrid nanostructures in combination with other compositions were reported to exhibit enhanced electrochemical performance in batteries and supercapacitors [34–37]. However, the main drawbacks of Co, which limit its utilization in energy storage devices including high cost, relatively low discharge current, poor cyclic stability and narrow potential window *etc.*. [38–40] Developing mixed metal oxide chemistries has been identified as a potential solutions to these above mentioned issues. The presence of various metal sites in the lattice has been shown to improve charge storage capability due to the synergetic effect of different metal cations present in the crystal lattice while decreasing the overall cost of the product. Ternary transition metal oxides may present the high specific capacitance relative to their single or binary metal oxide owing to their high electrical conductivity and synergetic effect, which facilitates the charge transport at electrode/electrolyte interface. Luo *et al.* synthesized Mn–Ni–Co oxide composite expressing the specific capacitance of 1260 Fg^{-1} [41]. Another research group Jae-Jin Shim *et al.* reported the synthesis of Fe–Ni–Co nanoflakes on nickel foam with the specific capacitance of 867 Fg^{-1} [42]. However, the electrochemical performance of the materials required to improve. Among all the ternary transition metal oxides, only a few reports were related to iron-nickel cobalt oxide used in supercapacitors application.

In this work, we synthesized novel morphology for mesoporous iron-nickel cobalt oxide nanowires (FNCO NWs) by a simple hydrothermal route followed by thermal treatment. The developed FNCO NWs exhibit much higher surface area and particulate morphology which leads to a higher electrode/electrolyte interface, thus leading to an enhanced electrochemical response. The developed FNCO NWs exhibit excellent specific capacitance of 2195 Fg^{-1} at current density of 1 Ag^{-1} with excellent stability for over 20,000 cycles in three electrode configuration. Such improvements in the electrochemical properties maybe attributed to the higher charge storage capacity, greater electrical conductivity and the active site density imparted by Ni and Fe additions [43,44]. Motivated by the excellent capacitive response, the asymmetric device was also fabricated using FNCO NWs and graphene as positive and negative electrodes, respectively. The assembled device exhibited excellent specific capacitance and energy density (47 $Whkg^{-1}$ at corresponding power density of 375 Wkg^{-1}) as well as high stability of 86% capacitance retention after 15,000 cycles.

2. Experimental section

2.1. Materials

All reagents utilized in this work were of analytical grade and employed without any further purification. Nickel nitrate hexahydrate ($Ni(NO_3)_2.6H_2O$), Urea ($CO(NH_2)_2$), Ammonium fluoride (NH_4F) and Iron nitrate nonahydrate ($Fe(NO_3)_2.9H_2O$) were purchased from Daejung Co. Ltd., South Korea. Cobalt nitrate hexahydrate ($Co(NO_3)_2.6H_2O$) was obtained from Unichem Inc. NC, USA, whereas the solvents i.e. Absolute ethanol (C_2H_5OH), isopropanol ($CH_3CHOHCH_3$) and nafion@perfluorinated resin solution were supplied by Sigma-Aldrich, MI, USA.

2.2. Synthesis

The FNCO NWs synthesis was carried out by a hydrothermal reaction between precursor chemicals in a reactor followed by air annealing of the solid product in a furnace. Then, 7.2765 g of $Co(NO_3)_2.6H_2O$ (25 mM), 3.63487 g of $Ni(NO_3)_2.6H_2O$ (12.5 mM), 5.05 g of $Fe(NO_3)_2.6H_2O$ (12.5 mM), 3.003 g of $CO(NH_2)_2$ (50 mM) and 0.5555 g of NH_4F (15 mM) were completely dissolved in 50 mL deionized (DI) water via magnetic stirring for 1 h. This homogeneous solution was then transferred to the stainless steel autoclave and treated at 130 °C for 7 h. The solution chemistry and the hydrothermal conditions were derived from a combination of extensive literature review and initial experimental runs. After hydrothermal treatment, the autoclave was air-cooled to room temperature to extract the precipitates. The reaction product was washed several times with ethanol and DI water several times, followed by filtration. Filtrated material was dried in an oven at 80 °C for 6 h and subsequently annealed in a furnace by heating at 1.5 °C/min to 400 °C and 2 h dwell time. After annealing, a dark brown colored powder was obtained which was stored in a vacuum desiccator for later use. Various synthesis steps of FNCO NWs have been schematically illustrated in Fig. 1. For comparison iron cobalt oxide (FCO), nickel cobalt oxide (NCO) and cobalt oxide (CO) were synthesized by same route.

2.3. Assembly of asymmetrical supercapacitor

The asymmetric supercapacitor was assembled by combining FNCO NWs as positive and graphene as a negative electrode. For this purpose, FNCO NWs and Nafion solution were added to the ethanol with a ratio of 90:10 followed by ultrasonic homogenization for 80 min. Over conducting electrode, the above suspension was gradually dropped, followed by vacuum oven drying for 60 min. The negative electrode was fabricated by the addition of graphene to N-Methyl-2-Pyrrolidone (NMP) and sonication, by further addition of Nafion solution as a binder. After complete homogenization, the suspension was poured over conducting electrode dropwise and dried in oven for 100 min. After making these electrodes, a whatman filter paper (grade 41; Sigma-Aldrich, USA) was used as a separator between the electrodes.

2.4. Characterizations

The morphology of the FNCO and graphene electrode materials was investigated using a high-resolution analytical transmission electron microscope (TEM) (FEI Tecnai F30; Thermo Fisher Scientific, MA, USA) and scanning electron microscope (SEM) (JEOL JSM6490A, Japan). The selected-area electron diffraction (SAED) and high resolution TEM (HR-TEM) analysis were also performed using TEM. The elemental composition and oxidation states of the elements were determined by means of an x-ray photoelectron spectroscope (XPS) (Kratos Axis Ultra; Kratos Analytical Ltd, UK) with monochromatic Al-Kα radiation (1486.6 eV). The x-ray diffraction (XRD) analysis (STADI MP; STOE & Cie GmbH, Germany) was carried out at 40 kV accelerating voltage and 40 mA emission current to study phase composition and structure of the

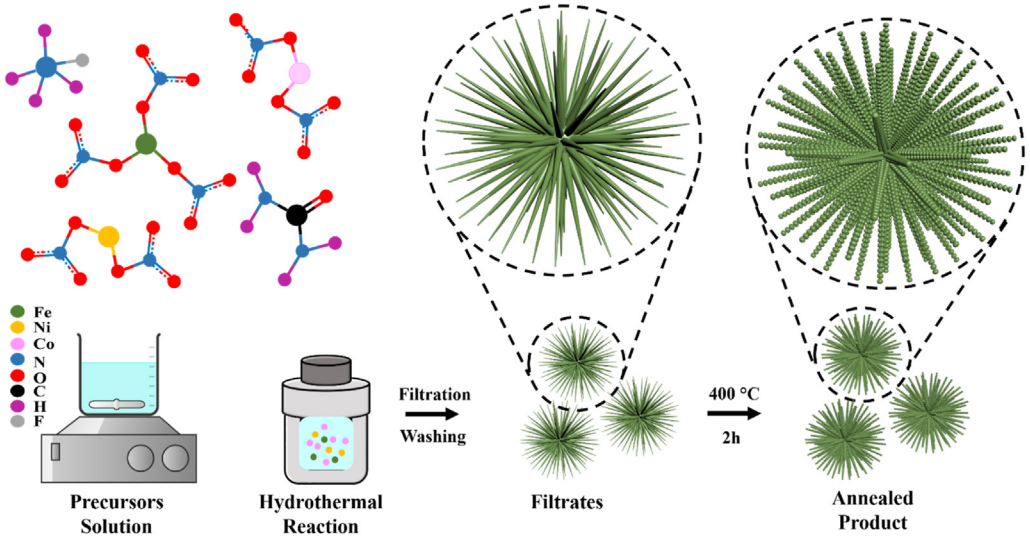

Fig. 1. Schematic illustration of the synthesis process of FNCO NWs. A homogenous solution of precursors is prepared by magnetic stirring at room temperature. Hydrothermal reaction produces needle like structure which are then heat treated obtain hierarchically mesoporous FNCO NWs.

synthesized nanostructures. The surface area of the FNCO NWs was determined using Gemini VII 2390 V1.03 BET surface area analyzer (Micromeritics Instrument Corp., GA, USA) after drying and degassing of the samples at 320 °C for 3 h to remove moisture and organic components. The electrochemical properties of the synthesized materials were carried out on a potentiostat (VSP-300; Bio-Logic Science Instruments, France). For this purpose, a 3-electrode configuration with FNCO NWs or graphene-coated glassy carbon, platinum (Pt) wire and Ag/AgCl as working electrode, a counter electrode and reference electrode, respectively was used. The working electrode was made by drop casting a stable suspension of electrode material and Nafion solution in ethanol over glassy carbon electrode (GCE) (Diameter 3 mm) and drying at 60 °C. The active mass 10 μg was deposited on GCE for testing. The cyclic voltammetry (CV) experiments were performed at scan rates of 10–100 mVs^{-1} with operating potential window of − 0.1 to 0.5 V. Also, galvanostatic charge-discharge (GCD) tests were carried out at current densities in the range of 1–20 Ag^{-1}. The electrochemical impedance spectroscopy (EIS) studies were executed in 6 M KOH solution at frequencies from 100 mHz to 1 MHz. The electrochemical testing of asymmetric supercapacitor was caaried out in two electrode assembly. All the tests were performed at wide operating potential window of 0 V–1.5 V.

3. Results and discussion

The schematic for the synthesis of the mesoporous FNCO NWs is presented in Fig. 1. First, under a facile hydrothermal reaction at 130 °C for 7 h, the raw materials react and form the precursor for the mesoporous FNCO NWs. Then the precursor for FNCO NWs was calcined in air ambient furnace at 400 °C for 2 h and resulted in the formation of high density mesoporous FNCO NWs. The detailed mechanism for the formation of FNCO NWs is described in the supporting information file.

The SEM examination of the FNCO NWs samples revealed the evolution of flower-like morphology from the arrangement of several nanowires, as indicated by low and high magnification microstructures presented in Fig. 2a-b. The flowerlike features appear to have a nodular shape with an apparent diameter of the order of 10 μm. Magnified SEM image of the individual features further revealed petal-like morphology with each petal comprising of numerous thin, nanowires that were oriented in the same direction and were several micrometers long and ~20–30 nm in diameter. The interconnected particulate morphology at nanoscale is expected to not only improve the surface area but also provide fast mass diffusion under higher current densities, which will promote the high rate capability of the developed product. Furthermore, the presence of open spaces could accommodate any volume changes during reversible cycling, thus improving the overall cyclic stability of the product. Further, SEM analysis was performed for CO, FCO and NCO to visualize the microstructures as shown in Figures (S1eS3) of supporting information. The phase analysis of the prepared nanostructures was done using XRD patterns, as shown in Fig. 2c. These patterns for the FNCO, FCO, NCO and CO coincide with JCPDS Card No. 01-080-1542 [45], thereby confirming the formation of Co_3O_4 cubic type structure. In case of CO characteristic diffraction peaks were positioned at 2-theta values of 19.11°, 31.29°, 36.79°, 44.71°, 55.56°, 59.29°, 65.17° and 77.31° corresponding to the (111), (220), (311), (400), (422), (511), (440) and (533) planes, respectively. The XRD patterns of NCO, FCO and FNCO resembled with pure Co_3O_4 sample, confirming the successful addition of Fe or/and Ni into the Co_3O_4 lattice without the formation of any additional phase. A slight shift in the peak positions was noticed in case of the NCO, FCO and FNCO samples as compared to the pure Co_3O_4, owing to the difference in ionic radii and electropositivity of the Fe^{2+}, Fe^{3+}, Ni^{2+}, Ni^{3+}, Co^{2+} and Co^{3+} ions. The cationic substitution causes lattice strain in the crystal structure of Co_3O_4 with associated changes in the position of the planes and the interplanar spacing values.

The morphology of FNCO NWs was further investigated using TEM studies. The TEM analysis revealed that the FNCO NWs are formed of much smaller rod like nanoparticles (~40–50 nm) which is consistent with the SEM analysis (Fig. 2d). The polycrystalline structure of FNCO NWs was also confirmed from the TEM analysis. From the HR-TEM analysis (Fig. 2e), the interplaner spacing was computed to be 0.246 nm, which corresponds to that of the (311) plane of the FNCO NWs. It was observed that (311) is the predominant crystallographic orientation in the FNCO samples. The existence of other directions is also evident from SAED pattern that comprised of concentric rings with an interplanar spacing of 0.475, 0.290, 0.245, 0.206, 0.168 and 0.146 nm that were indexed to be (111), (220), (311), (400), (511) and (440) planes, respectively as

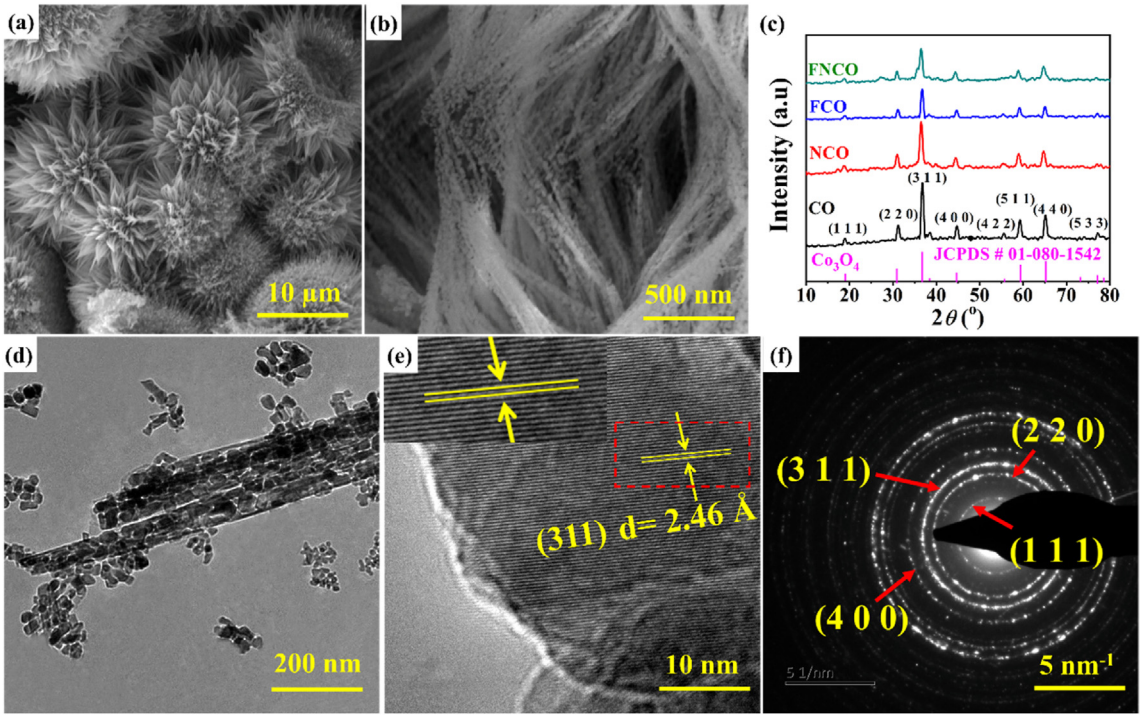

Fig. 2. (a) Low resolution SEM image of FNCO NWs, (b) High resolution SEM image of FNCO NWs (c) XRD pattern of FNCO NWs, NCO, FCO and CO, (d) TEM image of FNCO NWs (e) HR-TEM image of FNCO NWs (f) SAED image of FNCO NWs.

shown in Fig. 2f. The findings from HR-TEM and SAED studies are in good agreement with the XRD data and confirmed successful replacement of the cobalt cations with iron and nickel cations during the hydrothermal synthesis of the FNCO NWs.

X-ray photoelectron spectroscopy (XPS) was carried out to develop a thorough understanding of the chemical composition and oxidation states of the elements forming FNCO NWs. The universal survey spectrum of FNCO NWs showed the presence of Fe, Ni, Co and O, as presented in Figure S4; supplementary information. The high resolution XPS spectra for Fe, Ni, Co, and O, after deconvolution using Shirley background, are shown in Fig. 3a-d. There were two Co 2p peaks with energy states of Co $2p_{3/2}$ and Co $2p_{1/2}$ at respective binding energy (B.E.) values of 779.9 and 795.05 eV confirming the presence of both Co^{3+} and Co^{2+} ions, as labeled in Fig. 3a [46]. Similarly, the deconvolution of $Fe_{3/2}$ peak reveals the existence of Fe^{2+} and Fe^{3+} cations in the lattice (Fig. 3b) [47]. In Fig. 3c, the presence of both Ni $2p_{3/2}$ and Ni $2p_{1/2}$ XPS component peaks centered at 855.387 and 873.233 eV was attributed to Ni^{2+} and Ni^{3+} upon deconvolution of high resolution [48], whereas the shoulder peaks hinted at some degree of CoNi intermetallic compound formation. Deconvolution of the O1s XPS peak indicated three distinct component peaks at 529.5, 529.8 and 531.3 eV, as demonstrated in Fig. 3d.

The X-ray fluorescence (XRF) analysis of the FNCO NWs was carried out to determine elemental and molar compositions as shown in Figure S5. The quantitative analysis yielded the molar ratio of Fe, Ni and Co to be 23.08, 28.37 and 48.54, respectively. The values obtained are in close proximity of the initial molar ratio chosen for the hydrothermal synthesis and are a testament to the optimal processing conditions for the reaction between species for FNCO formation. Both surface area and inherent porosity of an electrode material play a key role in electrochemical performance. The pore width *vs.* pore volume plot and N_2 adsorption isotherm for FNCO NWs are shown in Figure S6. The FNCO NWs exhibited high BET surface area of 56 m^2g^{-1} which is much higher than CO and FCO presented in Table S1. The increase in surface area can be attributed to the creation of large spaces between agglomerated particles in FNCO NWs, which provides a large surface for N_2 adsorption. Furthermore, the FNCO NWs exhibited porosity in the mesoporous range (~8 nm), which is necessary to maintain fast mass diffusion under higher current densities.

The capacitive behavior of all the materials was studied in a voltage range of −0.1 V–0.5 V using 6 M KOH solution as an electrolyte in three electrode testing system. The cyclic voltammetry (CV) was performed at scan rates of 10 mVs^{-1}, 20 mVs^{-1}, 50 mVs^{-1} and 100 mVs^{-1} individually for comparison between CO, NCO, FCO, and FNCO NWs. The cyclic voltammogram for FNCO NWs, NCO, FCO and CO at different scan rates is shown in Figure S7.; which exhibits the highly responsive nature of FNCO NWs in comparison to other nanostructures. The CV curves for all materials were non-rectangular which affirmed the pseudocapacitive nature of materials. The CV study showed that the rise in scan rate caused to enhance the current produced in cyclic voltammogram, which revealed its highly capacitive properties of the material [49].

The GCD was performed to further study the electrochemical properties of FNCO NWs at different current densities. The specific capacitance of material was calculated through the GCD profile by using the formula [50,51]:

$$C_{sp} = \frac{I \times t}{m\Delta V}$$

Here I is a constant current in Amperes, t is discharge time in seconds, m is mass of active material deposited in gram and ΔV is a potential window. It is quite clear that the discharge time for FNCO NWs is much higher in comparison to other products as shown in Fig. 4a. Thus, the FNCO NWs exhibited a high specific capacitance of 2197 Fg^{-1} at the current density of 1 Ag^{-1}, which is tremendously higher than NCO (1213 Fg^{-1}), FCO (441 Fg^{-1}) and pure CO (251 Fg^{-1}). The higher capacitance can be attributed to the synergetic effect of

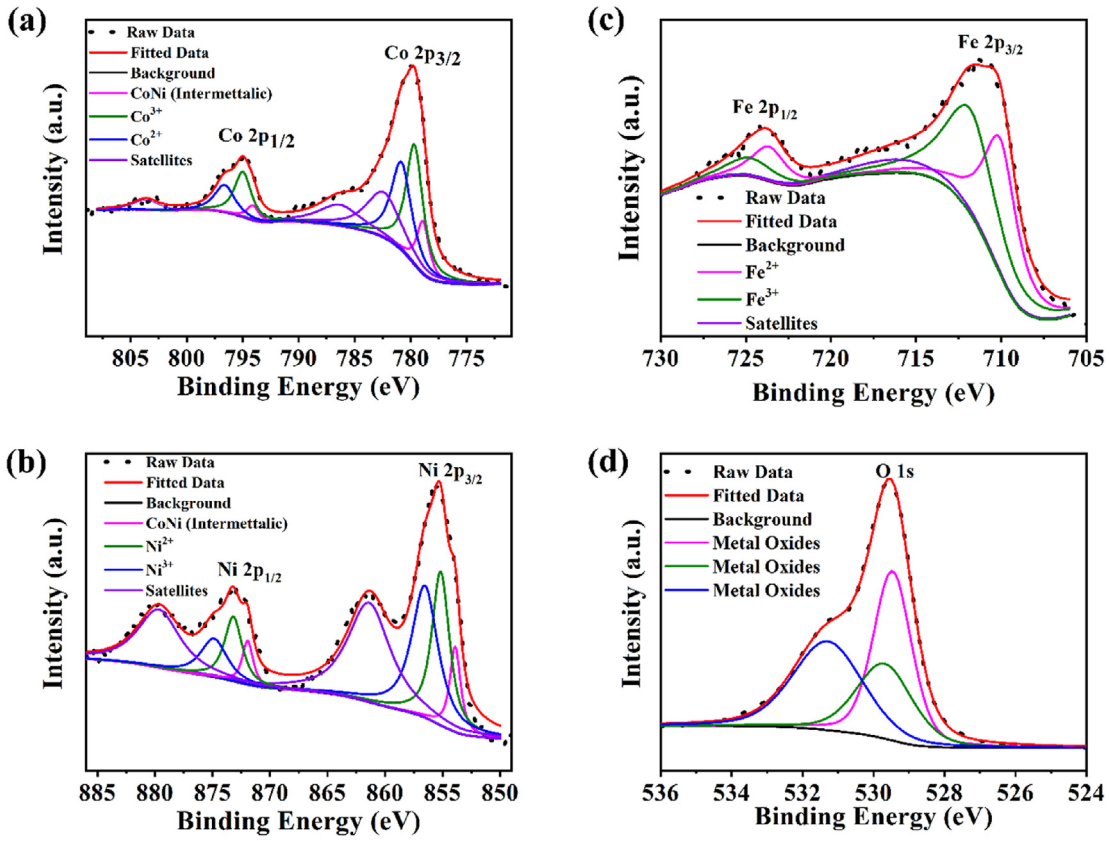

Fig. 3. High resolution XPS spectra of FNCO for (a) Co 2p (b) Fe 2p (c) Ni 2p and (d) O 1s.

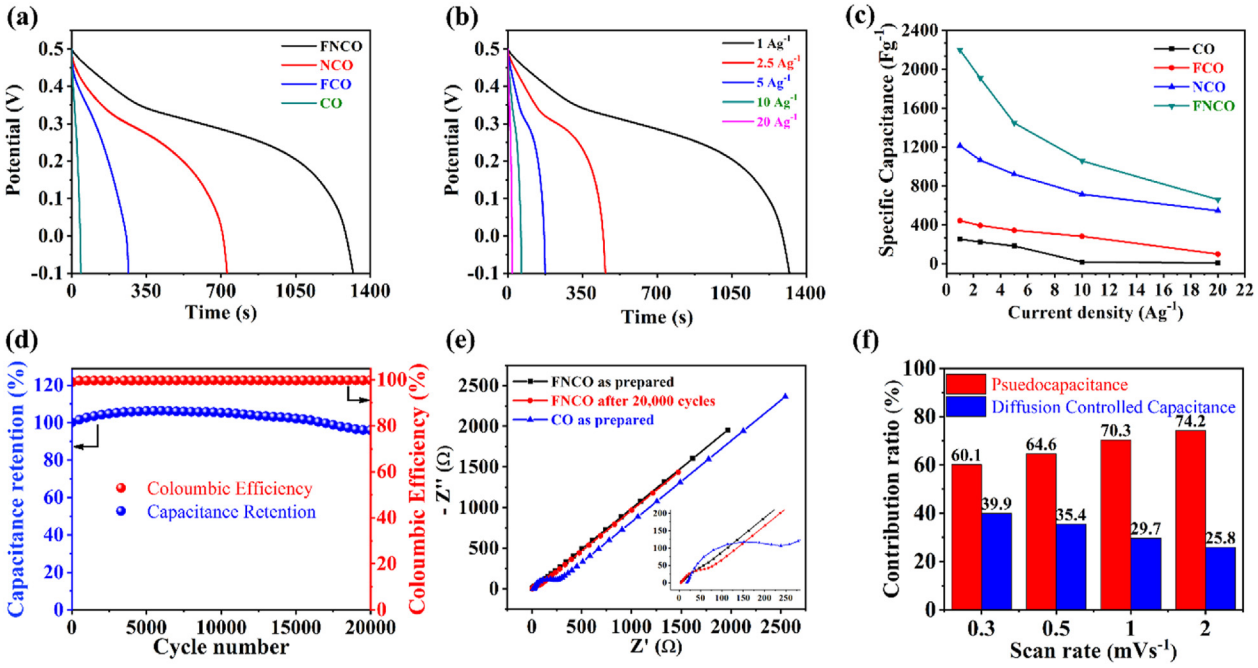

Fig. 4. (a) Discharge curves for FNCO NWs, NCO, FCO and CO performed at current density of 1 Ag^{-1} (b) Discharge curves for FNCO NWs performed at different current densities (c) Comparison between specific capacitance of CO, FCO, NCO and FNCO NWs calculated by GCD at different current densities (d) Comparison between coloumbic efficiency and capacitance retention of FNCO NWs in 6 M KOH solution for 20,000 GCD cycles (e) Nyquist plot of CO and FNCO NWs as prepared and FNCO NWs after 20,000 GCD cycles (f) Pseudocapacitive and diffusion controlled charge storage contribution at different scan rates.

iron and nickel in addition to cobalt in FNCO NWs lattice. Fig. 4b shows the discharge curves for FNCO NWs at various current densities of 1 Ag^{-1}, 2.5 Ag^{-1}, 5 Ag^{-1}, 10 Ag^{-1} and 20 Ag^{-1}. It is quite clear that the discharge time for electrode material decreases with increasing current density. Further GCD profile for CO, NCO and FCO is shown in Figure S8. The FNCO NWs could deliver unprecedented capacitance of 658 Fg^{-1} at high current density of 20 Ag^{-1}. In comparison, the CO, FCO and NCO exhibit much lower capacitances at such high current densities as summarized in Fig. 4c. Table S2 shows the comparison between the energy density and power density of the synthesized materials at different current densities. FNCO NWs exhibited a maximum energy density 109 $Whkg^{-1}$ with a corresponding power density of 300 Wkg^{-1} at a current density of 1 Ag^{-1}. Apart from the high specific capacitance and energy density, long term cycle stability is an important parameter for electrode material to be used in practical supercapacitors applications. The FNCO NWs exhibited excellent cyclic stability up to 20,000 GCD cycles at the current density of 50 Ag^{-1}. FNCO NWs revealed an impressive performance of charge stability by expressing capacitance retention up to 96% over 20,000 cycles of charge and discharge process as shown in Fig. 4d. Figure S9 shows the GCD curves for few cycles observed in process of 20000 cycles for FNCO NWs. Further, EIS was performed to study the charge transfer properties of synthesized electrode materials and resulted Nyquist plots are presented in Fig. 4e. CO showed a high charge transfer resistance up to 168 Ω which hinders it to be used as electrode material in supercapacitors. The addition of Ni and Fe ions in the structure of Co_3O_4 reduces the charge transfer resistance and the resulting FNCO NWs exhibited a low charge transfer resistance of 11 Ω which is much lower in comparison to CO. As with the passage of time the material reduces its efficiency, we also analyzed the charge transfer resistance of FNCO NWs after 20,000 GCD cycles. The FNCO NWs showed 33.03 Ω charge transfer resistance after 20,000 GCD cycles which clearly show minimal loss of conductivity over long cycling life, shown in Fig. 4e. Nyquist plot for CO, FCO and NCO and calculated charge transfer resistances are shown in Figure S10 and Table S3. In order to gain more information about the electrochemical charge storage behavior of the material the cyclic voltammetry was performed at low scan rate after complete activation of the process as shown in Figure S11 (a). It was clearly seen the presence of anodic and cathodic peaks in the cyclic voltammogram. log (i) vs log (v) was plotted as shown in Figure S11 (b) to evaluate the contribution of charge storage mechanisms using method previously reported in litrature [52,53] and quantified results are shown in Fig. 4 (f).

Motivated by the excellent capacitive response of FNCO NWs in three electrode configuration, aqueous asymmetric supercapacitor device was also assembled using FNCO NWs as positive electrode and a graphene based negative electrode. The structural and morphological analysis of used graphene sheets via XRD and SEM are given in Figures (S12eS13), respectively. The positive and negative electrode were gravimetrically balanced ($m_+/m_- = 0.5$) to achieve the maximum potential window. According to CV graph calculated through the three-electrode system in 6 M KOH solution, it is possible to expand the potential window up to 1.5 V for two electrodes asymmetric devices as shown in Fig. 5a. Fig. 5b shows the cyclic voltammetry curves for FNCO//Graphene asymmetric device calculated at different scan rates in 6 M KOH electrolyte. The device exhibited a significant change in the cyclic voltammetry curve with increasing the scan rate. In further studying the device characteristics, we performed GCD storage technique at different current densities to observe the response of the device. Fig. 5c shows the GCD curves for the asymmetric device at a current density of 0.5 Ag^{-1}, 1 Ag^{-1}, 1.5 Ag^{-1}, 2 Ag^{-1} and 5 Ag^{-1}. The specific capacitance calculated from these curves were 151.7 Fg^{-1}, 127 Fg^{-1}, 113.6 Fg^{-1}, 103 Fg^{-1} and 98.9 Fg^{-1}, respectively. The higher value of specific capacitance of FNCO//G device was achieved at a current density of 1 Ag^{-1} due to high charge storing and faradaic reaction

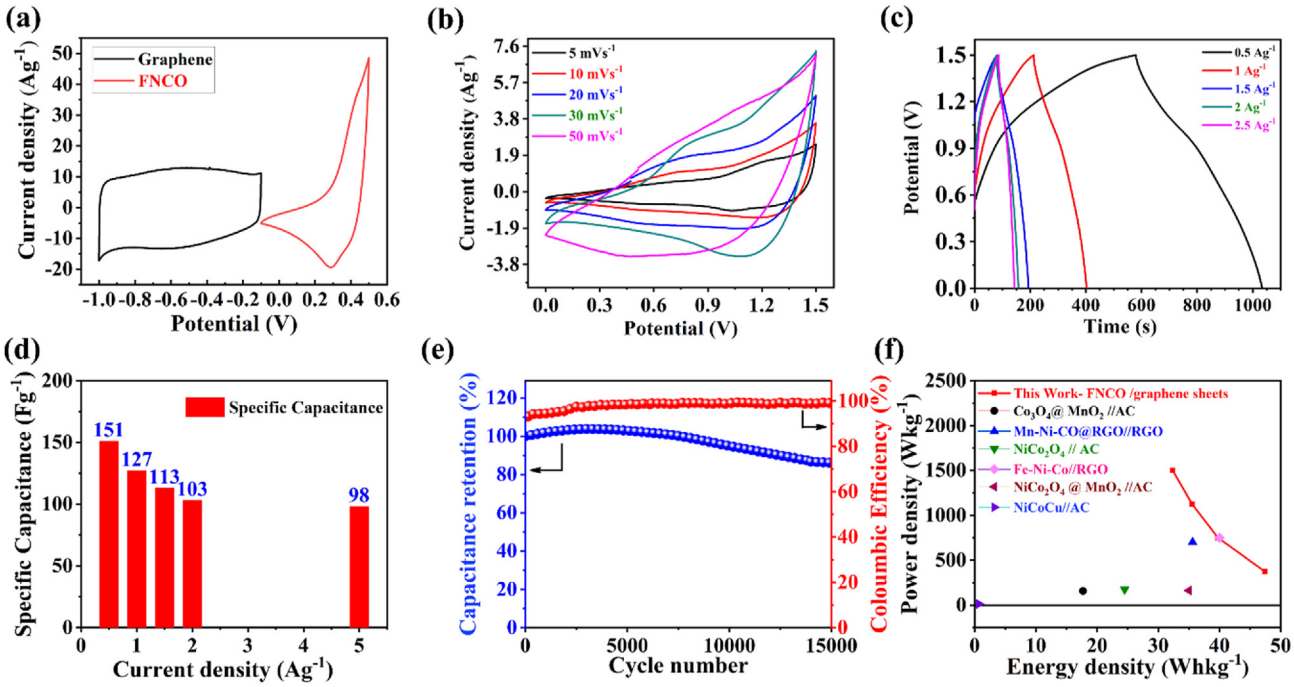

Fig. 5. (a) CV curve of graphene and FNCO at scan rate of 10 mVs^{-1} (b) Cyclic Voltammogram of asymmetric device at different scan rates (c) GCD graph of asymmetric device at different current densities (d) Specific capacitance of FNCO//graphene asymmetric device (e) Comparison between coloumbic efficiency and capacitance retention of asymmetric device (f) Ragone plot of FNCO//graphene asymmetric device (this work), Co_3O_4@MnO_2//AC [54], Mn–Ni–CO@RGO//RGO [55], $NiCo_2O_4$//AC [56], Fe–Ni–Co//RGO [42], $NiCo_2O_4$@MnO_2//AC [57], NiCoCu//AC [58].

capabilities of FNCO NWs deposited on the positive electrode shown in Fig. 5d, where it can be seen that the capacitance slightly decreases with increasing current density. The charging and discharging wings are approximately identical to each other, which reveals the best charge reversibility and coloumbic efficiency of the device. The FNCO//G device showed the capacitance retention of 86% after 15,000 GCD cycles as shown in Fig. 5e. The morphology and microstructure of the electrodes after cycling tests was evaluated again and the SEM results as shown in Figure S14 affirmed that the FNCO NWs were stable after 15000 charge/discharge cycles due to its unique composition and microstructure. This stability of FNCO NWs has helped in charge retention for a large number of cycles. And this remarkable performance compared with literature as given in Table S4 endorsed suitability of FNCO NWs for practical applications. Furthermore, the energy density and power density were calculated based on active material deposited on the electrode using the following equations.

$$E = \frac{1}{2} C_{sp} \Delta V^2$$

$$P = \frac{E}{t}$$

Here E is energy density and P is power density achieved by the device based on active electrode materials, C_{sp} specific capacitance, ΔV is operating potential window and t is discharging time. The FNCO//G exhibited an excellent energy density of 47 $Whkg^{-1}$ at the corresponding power density of 375 Wkg^{-1}. The power densities and corresponding energy densities of FNCO//G device are summarized in Fig. 5f.

4. Conclusion

Ternary oxide nanowires based on Fe, Ni and Co were synthesized through the facile hydrothermal route followed by a post-annealing treatment to achieve better crystallinity. High specific capacitance and energy density were achieved by this synthesized material due to its higher surface area, well-arranged wires morphology, structural stability and synergistic contributions of the individual components. FNCO showed higher capacitance 2197 Fg^{-1} which was significantly higher than binary and unitary oxid (NCO, FCO and CO) synthesized through the same route. In addition, the material demonstrated good long-term cyclic stability and low resistance studies by electrochemical impedance spectroscopy. Further, FNCO electrode was integrated with graphene nanosheets in the asymmetric device, resulting in a high energy density of 47 $Whkg^{-1}$ and a maximum power density of 375 Wkg^{-1}. Moreover, FNCO/graphene hybrid device showed an excellent rate capability at various current densities and cycling stability over 15,000 cycles. These results suggest that the prepared FNCO could be a superior candidate as an electrode material for the fabrication of highly efficient energy storage devices.

Declaration of competing interest

The authors declare that they have no known competing financial interests or personal relationships that could have appeared to influence the work reported in this paper.

Acknowledgments

This work is supported by the Higher Education Commission Pakistan Research Grant NRPU 9998.

Appendix A. Supplementary data

Supplementary data to this article can be found online at https://doi.org/10.1016/j.jmat.2021.03.012.

References

[1] Cao DH, Stoumpos CC, Farha OK, Hupp JT, Kanatzidis MG. 2D homologous perovskites as light-absorbing materials for solar cell applications. J Am Chem Soc 2015;137:7843–50.
[2] Deng J, Mortazavi M, Medhekar N, Zhe Liu J. Band engineering of Ni1 – xMgxO alloys for photocathodes of high efficiency dye-sensitized solar cells. J Appl Phys 2012;112:123703.
[3] Achour A, Islam M, Ahmad I, Saeed K, Solaymani S. Electrochemical stability enhancement in reactive magnetron sputtered VN films upon annealing treatment. Coatings 2019;9.
[4] Achour A, Lucio-Porto R, Solaymani S, Islam M, Ahmad I, Brousse T. Reactive sputtering of vanadium nitride thin films as pseudo-capacitor electrodes for high areal capacitance and cyclic stability. J Mater Sci Mater Electron 2018;29:13125–31.
[5] Liu J, Zhang J-G, Yang Z, Lemmon JP, Imhoff C, Graff GL, Li L, Hu J, Wang C, Xiao J, Xia G, Viswanathan VV, Baskaran S, Sprenkle V, Li X, Shao Y, Schwenzer B. Materials science and materials chemistry for large scale electrochemical energy storage: from transportation to electrical grid. Adv Funct Mater 2013;23:929–46.
[6] Usman M, Adnan M, Ali S, Javed S, Akram MA. Preparation and characterization of PANI@NiO visible light photocatalyst for wastewater treatment. Chemistry 2020;5:12618–23.
[7] Ali S, Javed S, Adnan M, Usman M, Akram MA. Synthesis and characterization of $CsPbBr_3$ for perovskite solar cells. Key Eng Mater 2021;875:3–9.
[8] Hassan A, Muhyuddin M, Rahman A, Usman M, Basit MA, Husain SW. Improved optical and electrochemical performance of MoS 2-incorporated TiO 2-PbS nanocomposite for solar paint application. J Mater Sci Mater Electron 2020;31:2625–33.
[9] Adnan M, Usman M, Akram MA, Javed S, Ali S, Ahmad I, Islam M. Study of magnetic and dielectric properties of ZnFe2O4/CoCr2O4 nanocomposites produced using sol-gel and hydrothermal processes. J Alloys Compd 2021:865.
[10] Huang M, Li F, Dong F, Zhang YX, Zhang LL. MnO 2-based nanostructures for high-performance supercapacitors. J Mater Chem 2015;3:21380–423.
[11] Wu N-L. Nanocrystalline oxide supercapacitors. Mater Chem Phys 2002;75:6–11.
[12] Salanne M, Rotenberg B, Naoi K, Kaneko K, Taberna PL, Grey CP, Dunn B, Simon P. Efficient storage mechanisms for building better supercapacitors. Nature Energy 2016;1:16070.
[13] Sun P, He W, Yang H, Cao R, Yin J, Wang C, Xu X. Hedgehog-inspired nanostructures for hydrogel-based all-solid-state hybrid supercapacitors with excellent flexibility and electrochemical performance. Nanoscale 2018;10:19004–13.
[14] Islam M, Javed S, Akram MA, Usman M. In: Advances in supercapacitor and supercapattery. Elsevier; 2021. p. 175–98.
[15] Usman M, Adnan M, Ahsan MT, Javed S, Butt MS, Akram MA. In situ synthesis of a polyaniline/Fe-Ni codoped Co3O4 composite for the electrode material of supercapacitors with improved cyclic stability. ACS Omega 2021;6:1190–6.
[16] Pendashteh A, Moosavifard SE, Rahmanifar MS, Wang Y, El-Kady MF, Kaner RB, Mousavi MF. Highly ordered mesoporous CuCo2O4 nanowires, a promising solution for high-performance supercapacitors. Chem Mater 2015;27:3919–26.
[17] Ma L, Chen S, Li H, Ruan Z, Tang Z, Liu Z, Wang Z, Huang Y, Pei Z, Zapien JA. Initiating a mild aqueous electrolyte Co 3 O 4/Zn battery with 2.2 V-high voltage and 5000-cycle lifespan by a Co (III) rich-electrode. Energy Environ Sci 2018;11:2521–30.
[18] Wang F, Wu X, Yuan X, Liu Z, Zhang Y, Fu L, Zhu Y, Zhou Q, Wu Y, Huang W. Latest advances in supercapacitors: from new electrode materials to novel device designs. Chem Soc Rev 2017;46:6816–54.
[19] Zhao C, Ren F, Xue X, Zheng W, Wang X, Chang L. A high-performance asymmetric supercapacitor based on Co (OH) 2/graphene and activated carbon electrodes. J Electroanal Chem 2016;782:98–102.
[20] Augustyn V, Simon P, Dunn B. Pseudocapacitive oxide materials for high-rate electrochemical energy storage. Energy Environ Sci 2014;7:1597–614.
[21] Ali Z, Asif M, Huang X, Tang T, Hou Y. Hierarchically porous Fe2CoSe4 binary-metal selenide for extraordinary rate performance and durable anode of sodium-ion batteries. Adv Mater 2018;30:1802745.
[22] Asif M, Rashad M, Ali Z, Qiu H, Li W, Pan L, Hou Y. Ni-doped MnO2/CNT nanoarchitectures as a cathode material for ultra-long life magnesium/lithium hybrid ion batteries. Materials Today Energy 2018;10:108–17.
[23] S. Kumar, G. Saeed, L. Zhu, K. N. Hui, N. H. Kim, J. H. Lee, 0D to 3D carbon-based networks combined with pseudocapacitive electrode material for high energy density supercapacitor: a review, Chem Eng J 2021, 403.
[24] Li L, Hui KS, Hui KN, Cho Y-R. Ultrathin petal-like NiAl layered double oxide/sulfide composites as an advanced electrode for high-performance asymmetric supercapacitors. J Mater Chem 2017;5:19687–96.
[25] Sun Z, Firdoz S, Yap EY, Li L, Lu X. Hierarchically structured MnO2 nanowires

supported on hollow Ni dendrites for high-performance supercapacitors. Nanoscale 2013;5:4379–87.
[26] Wang G, Tang Q, Bao H, Li X, Wang G. Synthesis of hierarchical sulfonated graphene/MnO2/polyaniline ternary composite and its improved electrochemical performance. J Power Sources 2013;241:231–8.
[27] Sarkar D, Khan GG, Singh AK, Mandal K. High-performance pseudocapacitor electrodes based on α-Fe2O3/MnO2 core–shell nanowire heterostructure arrays. J Phys Chem C 2013;117:15523–31.
[28] Maitra A, Das AK, Bera R, Karan SK, Paria S, Si SK, Khatua BB. An approach to fabricate PDMS encapsulated all-solid-state advanced asymmetric supercapacitor device with vertically aligned hierarchical Zn-Fe-Co ternary oxide nanowire and nitrogen doped graphene nanosheet for high power device applications. ACS Appl Mater Interfaces 2017;9:5947–58.
[29] Wu H, Lou Z, Yang H, Shen G. A flexible spiral-type supercapacitor based on ZnCo2O4 nanorod electrodes. Nanoscale 2015;7:1921–6.
[30] Xu L, Zhao Y, Lian J, Xu Y, Bao J, Qiu J, Xu L, Xu H, Hua M, Li H. Morphology controlled preparation of ZnCo 2 O 4 nanostructures for asymmetric supercapacitor with ultrahigh energy density. Energy 2017;123:296–304.
[31] Liu S, Ni D, Li H-F, Hui KN, Ouyang C-Y, Jun SC. Effect of cation substitution on the pseudocapacitive performance of spinel cobaltite MCo2O4 (M = Mn, Ni, Cu, and Co). J Mater Chem 2018;6:10674–85.
[32] Liu S, Yin Y, Ni D, Hui KS, Ma M, Park S, Hui KN, Ouyang C-Y, Jun SC. New insight into the effect of fluorine doping and oxygen vacancies on electrochemical performance of Co2MnO4 for flexible quasi-solid-state asymmetric supercapacitors. Energy Storage Materials 2019;22:384–96.
[33] Pendashteh A, Palma J, Anderson M, Marcilla R. Facile synthesis of NiCoMnO4 nanoparticles as novel electrode materials for high-performance asymmetric energy storage devices. RSC Adv 2016;6:28970–80.
[34] Xu W, Lyu F, Bai Y, Gao A, Feng J, Cai Z, Yin Y. Porous cobalt oxide nanoplates enriched with oxygen vacancies for oxygen evolution reaction. Nanomater Energy 2018;43:110–6.
[35] Ma F-X, Yu L, Xu C-Y, Lou XWD. Self-supported formation of hierarchical NiCo 2 O 4 tetragonal microtubes with enhanced electrochemical properties. Energy Environ Sci 2016;9:862–6.
[36] Yan N, Hu L, Li Y, Wang Y, Zhong H, Hu X, Kong X, Chen Q. Co3O4 nanocages for high-performance anode material in lithium-ion batteries. J Phys Chem C 2012;116:7227–35.
[37] Ahsan MT, Usman M, Ali Z, Javed S, Ali R, Farooq MU, Akram MA, Mahmood A. 3D hierarchically mesoporous zinc-nickel-cobalt ternary oxide (Zn0.6Ni0.8-Co1.6O4) nanowires for high-performance asymmetric supercapacitors. Front Chem 2020;8:487.
[38] Mei J, Liao T, Ayoko GA, Bell J, Sun Z. Cobalt oxide-based nanoarchitectures for electrochemical energy applications. Prog Mater Sci 2019;103:596–677.
[39] Chang B, Gu Z, Guo Y, Li Z, Yang B. Glucose-assisted synthesis of Co3O4 nanostructure with controllable morphologies from nanosheets to nanowires. J Alloys Compd 2016;676:26–36.
[40] He G, Li J, Chen H, Shi J, Sun X, Chen S, Wang X. Hydrothermal preparation of Co3O4@graphene nanocomposite for supercapacitor with enhanced capacitive performance. Mater Lett 2012;82:61–3.
[41] Luo J-M, Gao B, Zhang X-G. High capacitive performance of nanostructured Mn–Ni–Co oxide composites for supercapacitor. Mater Res Bull 2008;43:1119–25.
[42] Sahoo S, Nguyen TT, Shim J-J. Mesoporous Fe–Ni–Co ternary oxide nanoflake arrays on Ni foam for high-performance supercapacitor applications. J Ind Eng Chem 2018;63:181–90.
[43] Liu B, Liu B, Wang Q, Wang X, Xiang Q, Chen D, Shen G. New energy storage option: toward ZnCo2O4 nanorods/nickel foam architectures for high-performance supercapacitors. ACS Appl Mater Interfaces 2013;5:10011–7.
[44] Vialat P, Mousty C, Taviot-Gueho C, Renaudin G, Martinez H, Dupin JC, Elkaim E, Leroux F. High-performing monometallic cobalt layered double hydroxide supercapacitor with defined local structure. Adv Funct Mater 2014;24:4831–42.
[45] Feng Y, Sakaki M, Kim J-h, Huang J, Kajiyoshi K. Novel Prussian-blue-analogue microcuboid assemblies and their derived catalytic performance for effective reduction of 4-nitrophenol. New J Chem 2018;42:20212–8.
[46] Chuang T, Brundle C, Rice D. Interpretation of the x-ray photoemission spectra of cobalt oxides and cobalt oxide surfaces. Surf Sci 1976;59:413–29.
[47] Yamashita T, Hayes P. Analysis of XPS spectra of Fe2+ and Fe3+ ions in oxide materials. Appl Surf Sci 2008;254:2441–9.
[48] Chigane M, Ishikawa M. XRD and XPS characterization of electrochromic nickel oxide thin films prepared by electrolysis–chemical deposition. J Chem Soc, Faraday Trans 1998;94:3665–70.
[49] Heo JH, Han HJ, Kim D, Ahn TK, Im SH. Hysteresis-less inverted CH 3 NH 3 PbI 3 planar perovskite hybrid solar cells with 18.1% power conversion efficiency. Energy Environ Sci 2015;8:1602–8.
[50] Wu J, Zhang Qe, Zhou Aa, Huang Z, Bai H, Li L. Phase-separated polyaniline/graphene composite electrodes for high-rate electrochemical supercapacitors. Adv Mater 2016;28:10211–6.
[51] Chen T, Hao R, Peng H, Dai L. High-performance, stretchable, wire-shaped supercapacitors. Angew Chem Int Ed 2015;54:618–22.
[52] Ali Z, Tang T, Huang X, Wang Y, Asif M, Hou Y. Cobalt selenide decorated carbon spheres for excellent cycling performance of sodium ion batteries. Energy Storage Materials 2018;13:19–28.
[53] Zhang K, Park M, Zhou L, Lee G-H, Li W, Kang Y-M, Chen J. Urchin-like CoSe2 as a high-performance anode material for sodium-ion batteries. Adv Funct Mater 2016;26:6728–35.
[54] Huang M, Zhang Y, Li F, Zhang L, Wen Z, Liu Q. Facile synthesis of hierarchical Co3O4@ MnO2 core–shell arrays on Ni foam for asymmetric supercapacitors. J Power Sources 2014;252:98–106.
[55] Wu C, Cai J, Zhu Y, Zhang K. Hybrid reduced graphene oxide nanosheet supported Mn–Ni–Co ternary oxides for aqueous asymmetric supercapacitors. ACS Appl Mater Interfaces 2017;9:19114–23.
[56] Bhagwan J, Nagaraju G, Ramulu B, Sekhar SC, Yu JS. Rapid synthesis of hexagonal NiCo2O4 nanostructures for high-performance asymmetric supercapacitors. Electrochim Acta 2019;299:509–17.
[57] Xu K, Li W, Liu Q, Li B, Liu X, An L, Chen Z, Zou R, Hu J. Hierarchical mesoporous NiCo 2 O 4@ MnO 2 core–shell nanowire arrays on nickel foam for aqueous asymmetric supercapacitors. J Mater Chem 2014;2:4795–802.
[58] Sun H-Y, Lin L-Y, Huang Y-Y, Hong W-L. Nickel precursor-free synthesis of nickel cobalt-based ternary metal oxides for asymmetric supercapacitors. Electrochim Acta 2018;281:692–9.

Muhammad Usman is currently a PhD student at College of Engineering, Peking University China under the supervision of Dr. Yanglong Hou. Muhammad Usman recieved his MS degree in Nanoscience and Engineering in 2019 from National University of Sciences & Technology Pakistan. His research interests include synthesis of nano structures for electrode materials of Na ion batteries, Li ion batteries, supercapacitors and electrocatalytic water splitting.

Yiqiang Zhan, received his PhD degree in Physics from the department of physics, Fudan University, China, in 2005. He is currently serving as Professor and Director of Micro-Nano System Center at Fudan University, China. He won Shanghai Pujiang Scholar award in 2012. His current research interests include photovoltaic devices and LEDs based on organic-inorganic hybrid perovskite and organic semiconductor, flexible electronics, smart electronics and sensors.

Sajid Butt obtained his PhD degree in materials science and engineering from Tsinghua University China in 2015. He joined the institute of Space Technology Pakistan as Assistant Professor in 2015 on tenure track system. His current research interests include; thermoelectric materials, structure-property relationships, transport properties in materials, optoelectronic materials and·functional ceramics.

Muhammad Aftab Akram obtained BS degree in metallurgical and materials engineering in 2008 and PhD degree in Materials and Surface Engineering in 2017 from National University of Sciences & Technology Pakistan. He joined School of Chemical and Materials Engineering in 2017 as Assistant Professor. He was awarded Presidential Gold Medal in 2012 for academics and institutional best resaercher award in 2019. His research interests include electrode materials for supercapacitors, perovskite based solar cells, hybrid ion capacitors and photoelectrochemical water splitting.